Paper: ASAT-15-200-AE

15th International Conference on
AEROSPACE SCIENCES & AVIATION TECHNOLOGY,
ASAT - 15 – May 28 - 30, 2013, Email: asat@mtc.edu.eg ,
Military Technical College, Kobry Elkobbah, Cairo, Egypt,
Tel: +(202) 24025292 –24036138, Fax: +(202) 22621908

Experimental Investigation of Propeller Propulsion Model for a Small UAV Using Wind Tunnel

{A. M. Kamal*, A. M. Bayoumy, A. M. Elshabka}†

Abstract: Propulsion system modeling including propeller performance characteristics has a very important effect in the design and performance prediction of propeller-driven Unmanned Aerial Vehicles (UAVs). Motivated by modeling and simulation of small propeller-driven UAVs, the present paper focuses on the investigation of an accurate propeller-propulsion model used in these UAVs. First, propeller performance characteristics are measured in wind tunnel. Then, the engine model is identified based on experimental measurements of the engine input and output signals. The complete propeller-propulsion model, combining propeller and engine models, is then developed.

Aerodynamic tests are performed at a low speed subsonic wind tunnel to measure both propeller static and dynamic characteristics. A special test rig is designed and manufactured in which the engine, propeller and all sensors are mounted. The propeller dynamic test is conducted by changing the advance ratio. This can be done by changing either throttle position or wind tunnel airspeed while keeping the other one constant. Both ways are used to collect dynamic performance data which allow covering the whole range of advance ratios until reaching the braking and windmill modes. For each advance ratio, thrust, torque and power coefficients and hence the efficiency are obtained. For the propeller static test, thrust and torque are measured in stationary air over a range of propeller rotational speeds (RPM). The relation between the coefficient of thrust, torque, power and the static efficiency were obtained at a large range of RPM. The results show good agreement with published data. Engine and its servo motor is identified using experimental data as either first or second order transfer function model. The complete propeller-propulsion model is developed, validated with a very good agreement between simulation and experimental data.

Keywords: Propeller characteristics, propeller-driven UAV, propulsion system modeling and simulation, wind tunnel testing.

Nomenclature

CP	Coefficient of power.
CT	Coefficient of thrust.
D	Diameter of Propeller in meter.
J	Advance Ratio.
n	Propeller rotational speed measured in revolutions per second.
P	Propeller power.
Q	torque moment.
RPM	Propeller rotational speed measured in revolutions per minute.
T	Thrust force.
ρ	Density of air.

* ashrafkamal_85@hotmail.com .
† Egyptian Armed Forces, Egypt.

Introduction

Accurate investigation of UAV propulsion model plays a very important role to get a high fidelity complete nonlinear simulation model either for new designed UAV or to analyze an existing one. The accuracy of the propeller-propulsion model depends mainly on the propeller performance data, which also very crucial for selection of correct combination of engine and propeller in the design and performance prediction of UAVs. Due to the lack of propeller performance characteristics, several researches have been conducted in this area to gather information about these propulsion systems. Then, proper motor and propeller combinations can be selected for a given mission profile of UAVs. Kailash Kotwani., S.K. Sane., Hemendra Arya., K. Sudhakar. [1] establish a wind tunnel measurement system and obtain the performance maps for some mini/micro vehicles class propellers and engines. Robert W. Deters and Michael S. Selig [2] test the static performance for Eighteen two-blade and two three blades of micro propellers with small Reynolds numbers (less than 50,000) and diameters ranging from 2.25 in. to 5 in. A load cell and a torque transducer were used to measure thrust and torque, respectively concluding that propellers with a larger diameter are more efficient, and lower pitch for propellers of the same diameter are more efficient. The results of these twenty propellers provide a set of data can be compared against static performance prediction codes. John B. Brandt and Michael S. Selig [3] measure many propellers (79) of low Reynolds number range ($0.5\times10^5 - 1.0\times10^5$) to quantify the propeller efficiency at these conditions and examine low Reynolds number effects. The results showed significant Reynolds number effects with degradation in performance with lower RPM and create a large database for different types of propeller between 9-11inch diameters. Amer AI-Radaideh, M.A.AI-Jarrah, Ali Jhemi, and R.Dhaouadi [4] characterize the engine response to throttle command by assuming all inputs are constant and only the throttle is varied. Then by measuring engine thrust and the engine RPM, the transfer function that relates the throttle command to engine RPM and to the propeller thrust force obtained.

In this research, a propeller-engine-servo model is tested. Thrust and torque are measured over a range of discrete propeller speeds (RPM). Also, static thrust is measured for the same propeller-engine model. Then, by measuring the engine input and output signals, the engine model can be identified.

The remainder of this paper describes the experimental setup, propeller performance measurements, and identification of the engine model, presents results, discussion and finally the conclusion.

Experimental Setup

The objective of this experiment is to measure the performance characteristics of propeller from static conditions to the windmill state and modeling of the engine-propeller combinations. To do this, a special test rig was designed. The schematic of the experimental setup including the test bench and all equipment are presented in Fig. 1. The test was carried out inside a low speed subsonic wind tunnel, Fig. 2. The setup included a six-component strain gauge sting balance, engine, propeller and the fixation which connecting them to the sting balance with the required tolerance, RPM magnetic sensor connected with flight data recorder (FDR), throttle servo motor and all necessary transmitting and receiving devices, 5-volt battery, remote control (RC) transmitter and receiver, FDR transmitter, antenna and receiver, 3 pitot-static tubes averaged together, two Honeywell precision altimeter (HPA), National Instruments (NI) data acquisition system used to collect data from the instrumentation and a personal computer.

The experimental equipment allow for measuring a lot of parameters including the propeller thrust (N) and torque (N.m), the speed of the propeller (RPM), throttle position (%), static and total pressure (Pa) and temperature (^{o}C).

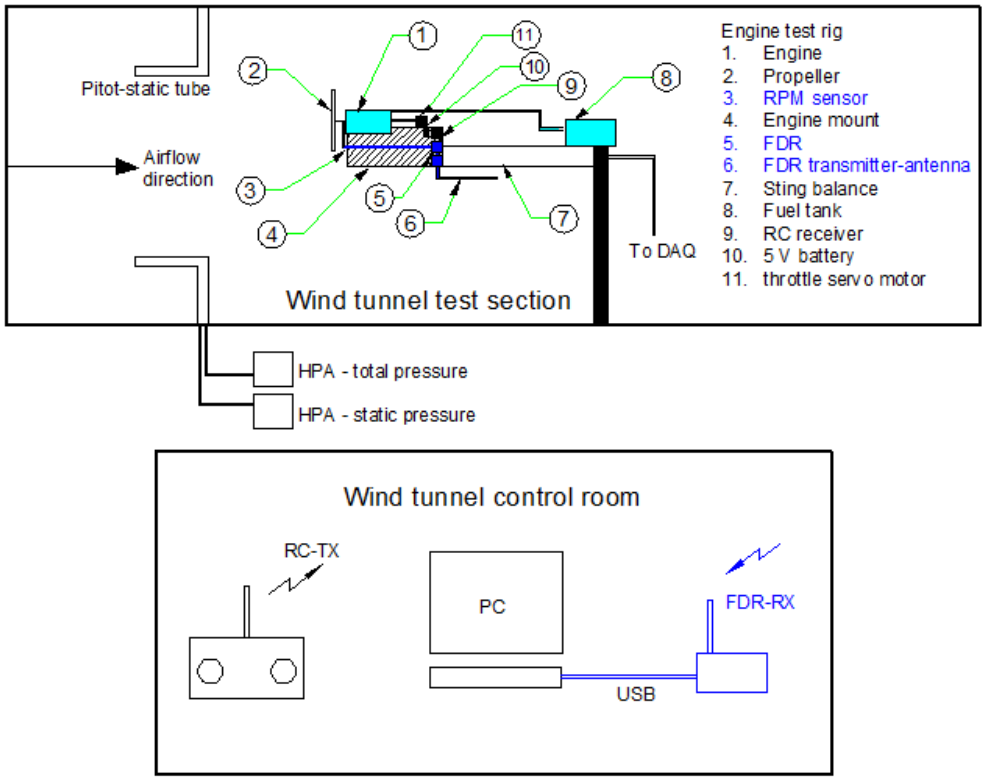

Fig. 1. The schematic of the test bench and equipment.

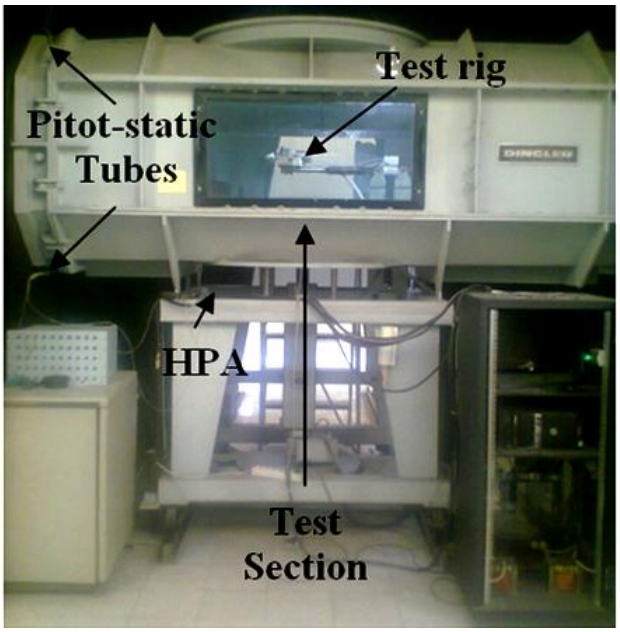

Fig. 2. Test rig installed inside the wind tunnel test section

Low Speed Wind Tunnel

The used Wind Tunnel (WT) is a closed circuit, low speed subsonic WT capable of producing a range of airspeeds from nearly (23) m/s up to nearly (52) m/s. It could have either open or closed test section. The test section shape is rectangular with tapered corners. The wind tunnel test section dimensions are: (1.15) m height, (1.5) m width and (3) m length. According to [6] the wind tunnel has low turbulence factor (by sphere drag method: τ_F=1.132 and by pressure sphere τ_F=1.2) and both results are in the normal limits which range from 1.0 up to 1.4, so the tunnel has acceptable turbulence in the closed test section. It has a 6-components strain-gauge sting balance. The wind tunnel has a 0.45 % maximum deviation of velocity at each point from that at the axis of the test section, so the tunnel has accepted uniform velocity profile distribution across the test section. Also, the ratio of the dynamic pressure at the test section and that at the outlet of the nozzle (called the wind tunnel constant) lies in the accepted limits. The graphical representation of the static pressure gradient (along the test section) and its dependence on the dynamic pressure is shown in Fig. 3. These results are in accord with the practical ranges.

So, it was concluded that the wind tunnel has a good and acceptable aerodynamic characteristics and the results obtained are accurate to a great extent.

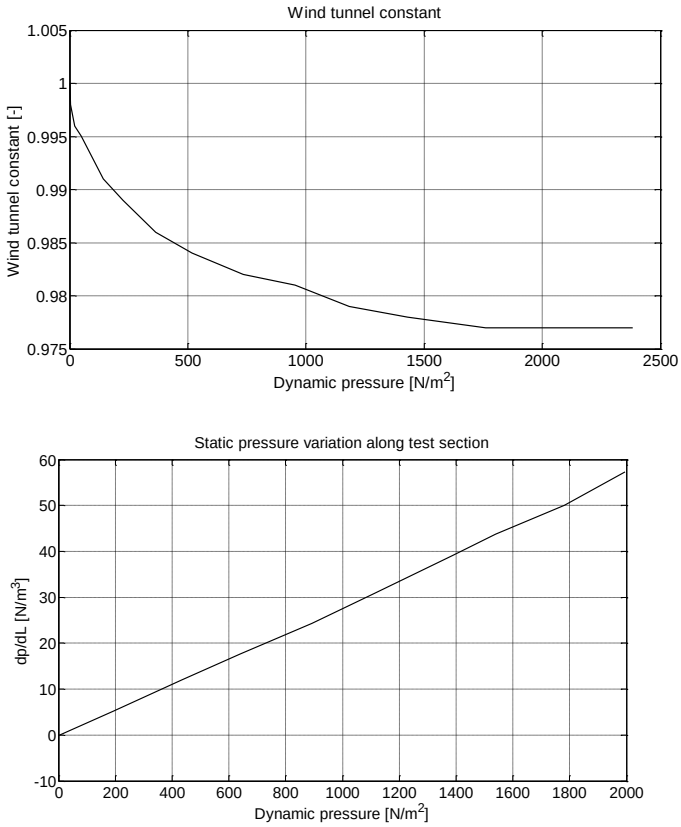

Fig. 3 Variation of wind tunnel characteristics with the dynamic pressure

Force and Moment Measurements

The thrust and torque produced by the propeller were measured using Aerolab 6 component strain gauge sting balance that shown in Fig. 4. The sting balance measures 6 loads (normal force1, normal force2, side force1, side force2, axial force and rolling moment). Strain gauges located in the Sting Balance are connected together with one cable with D-sub 25 connector.

Fig. 4 Aerolab 1 inch sting balance

The data acquisition system used to collect data from the sting balance consists of NI CompactDAQ cDAQ-9188 Chassis with 2x NI 9237 bridge modules connected to the PC through Ethernet. The NI 9237 strain gauge acquisition module provides the ability to measure a full and half bridge measurements simultaneously. Every strain gauge of the sting balance is connected to an RJ-50 connector that provides connections to four half or full bridges, and for external excitation voltage source. So, the D-sub connector has been connected to RJ-50 connectors for every strain gauge. The sting balance comes with a full bridge, 120 ohm strain gauge for each force/moment components. The NI 9237 card acquire the strain gauge signals and using Wind Tunnel (WT) software, the calibration matrix is applied to convert the micro-strain measurements to force/moment units.

Propeller Speed Control and Measurement

The propeller speed was controlled by sending a Pulse Width Modulation (PWM) signal from the RC transmitter to the RC receiver which is connected to Futaba S3010 servo motor with a mechanical connection to the engine. The number of revolutions of the output shaft was counted using EagleTree system. This system consists of one magnet, magnetic RPM sensor with range 100 RPM up to approximately 50000 RPM, flight data recorder (FDR), seagull transmitter to transmit the data from the test section and seagull wireless dashboard to receive the data in the control room. Installing the RPM sensor and magnets is the most challenging part of installation. First a suitable location on the engine was found to attach one small magnet and the RPM sensor. This location should ensure the magnets are mounted on some structure that does not “flop around” and the magnets don’t hit the sensor in rotation. The RPM sensor is mounted so that it does not move around, and it is within 1-2 mm of the magnet as it spins. To flush mount the magnets, a hole just slightly larger than the diameter of the magnet size was drilled with the same depth as that magnet, then the magnet was glued using epoxy. Then the RPM sensor was installed with a zip tie as shown in Fig. 5. The distance between the sensor and the magnet must be (1-2 mm). This distance has been established by putting a small spacer of 2 mm. Then the sensor connector was plugged into the FDR. The 900 MHz/200 mW Seagull Transmitter with its antenna were installed and connected to FDR. A Y-cable was used to feed the PWM signal from the receiver to the servo motor and to the FDR for recording the input throttle signal. A 5 volt battery with a Y-cable was used to power both the RC receiver and FDR. The Seagull Dashboard Receiver was connected to the PC with USB cable to power and allow live mode logging of the transmitted data.

Fig. 6 presents the block diagram of the used propeller speed sensors and control devices in both wind tunnel test section and control room while Fig. 7 shows these sensors as installed on the test rig.

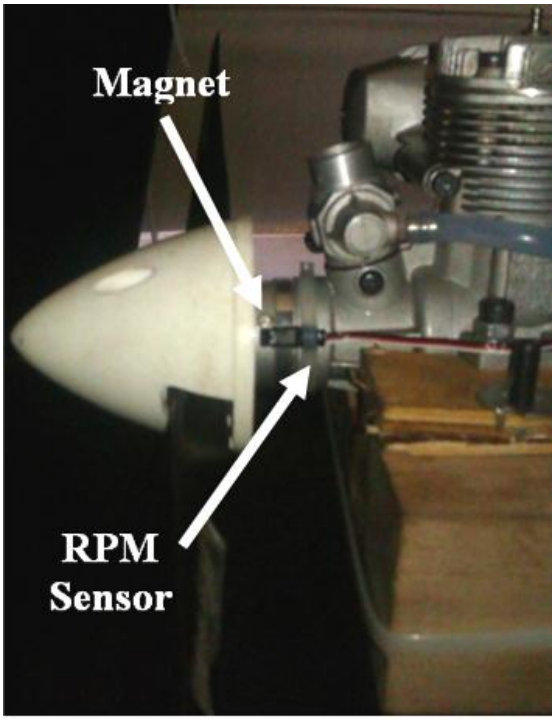

Fig. 5 Installation of RPM sensor and magnet

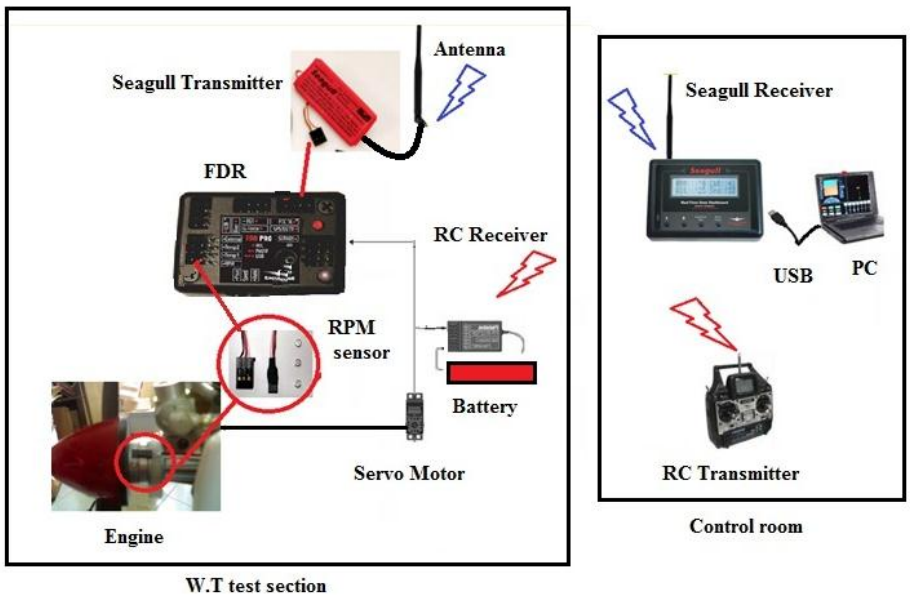

Fig. 6 Block diagram of the propeller speed sensors and control devices

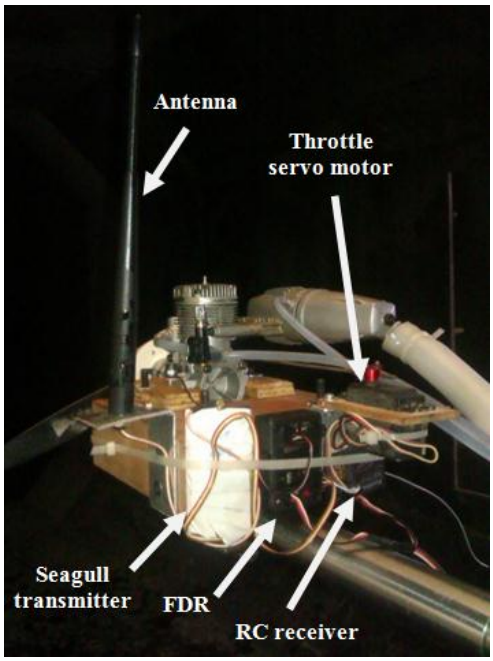

Fig. 7 Propeller speed sensors and control devices installed in the test rig

Wind Tunnel Speed Measurement

The wind tunnel speed was measured with a three pitot-static tube placed around the test section inlet as shown in Fig. 1. The total and static pressure lines were connected with two Honeywell Precision Altimeters (HPA200X2) for measuring pressure and temperature which provides high-accuracy absolute pressure readings in digital form. The HPA200X2 barometer measures air pressure up to: 121347.7 Pa ± 40 Pa max. The HPA interface with RS-232 enables receiving and sending data to a single serial port of a computer. The air density and the free stream velocity can be then calculated.

Propulsion System, Accessories and Engine Mount

The propeller that was tested is: Master Airscrew 11x6 G/F G3 Nylon Propeller. The geometric characteristics of the tested propeller can be estimated using the software package PropellerScanner [8] PropellerScanner tries to reconstruct the blade shape of a two bladed propeller by tracing front and side views presented in digital photos as shown in Fig. 8. The geometric data of the tested propeller are the chord length, blade twist and pitch distribution along the blade radius as shown in Fig. 9.

Fig. 8 Propeller front and side view digital photos

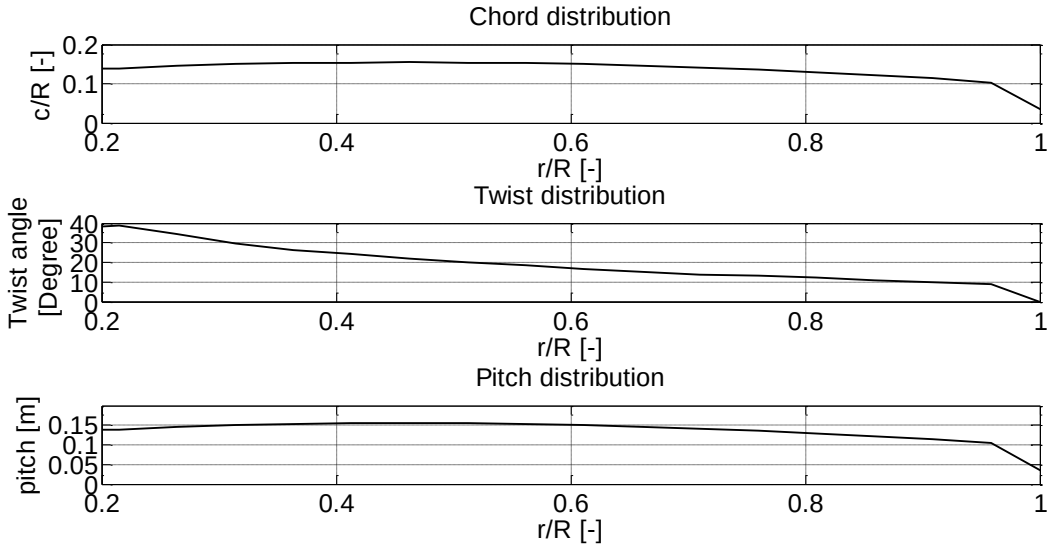

Fig. 9 Chord, twist and pitch distribution along the radius

The tested propeller is driven by a piston engine (O.S.Max-46AX) with the specification given in Table 1. The throttle position of the engine was controlled using: Futaba S3010 servo motor connected to the Futaba receiver.

Table 1 Engine specifications

Displacement	Bore	Stroke	Output power	RPM range	Suggested propeller sizes
7.45 cc/ 0.455 cu in.	22 mm/ 0.866 in.	19.6 mm/ 0.772 in.	1.65 hp @ 16000 rpm	2000-17000	10.5x6, 11 x6-8, 12 x6-7

To ensure accurate thrust and torque measurements, the fitting between the sting balance and test rig should be in the permissible tolerance ($1"^{-0.0005"}_{-0.0010"}$). A fixation adapter to the one inch Aerolab sting balance is designed and manufactured with this tolerance to be used with any wind tunnel model to ensure the required fitting as shown in Fig. 10.

To allow fixing the engine, propeller and all sensors to this adapter, a wooden engine mount is designed and manufactured to be connected to this adapter. To ensure continuous engine fuel feeding during the test, the fuel tank mounted in the same level of the test rig inside the test section. Finally the engine exhaust was diverted outside the test section using a hose. The assembly of all experiment apparatus inside the wind tunnel test section is shown in Fig. 11.

Propeller Performance Measurement

Methodology

To measure the propeller performance, the static and dynamic thrust and torque of the propeller are measured using the test rig mentioned in section 2. The strain gauge output signals are acquired by a National Instruments data acquisition board and a PC running custom-designed WT software for measuring the loads (thrust and torque). The WT software also used for sting balance signal calibration. The tunnel static and dynamic pressure,

temperature were measured using two Honeywell precision altimeter (HPA), then the free stream velocity and the air density calculated. The WT software collects the thrust and torque from the balance, static pressure, temperature and total pressure from the HPA and calculates density and velocity as follows.

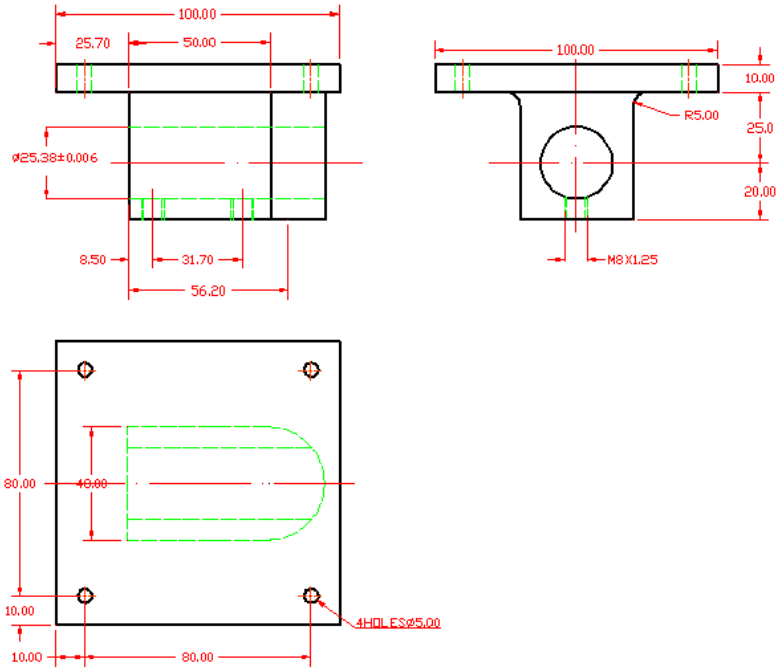

Fig. 10 Fixation adapter for connecting sting balance and test rig with dimensions in mm

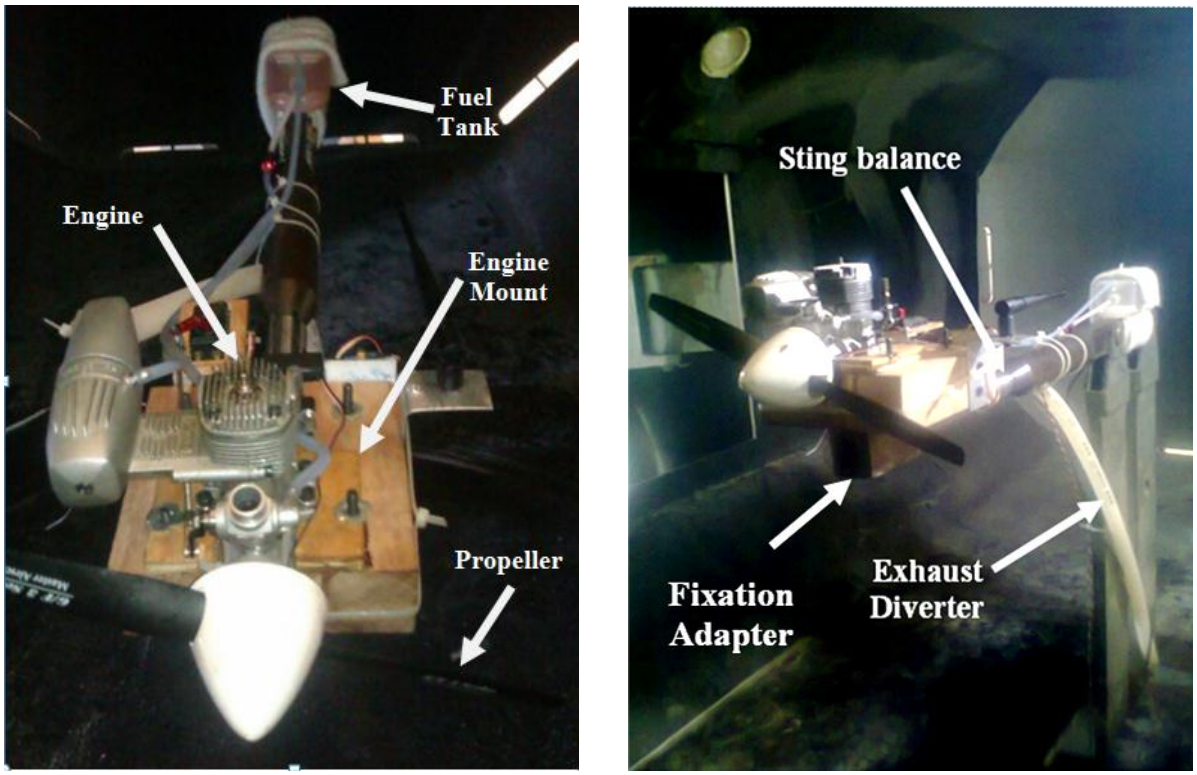

Fig. 11 All experiment apparatus

$$\rho = \frac{P_{static}}{RT} \quad , \quad R = 287.1 \ \frac{J}{kg.K}$$
$$V_{\infty} = \sqrt{\frac{2(P_{total} - P_{static})}{\rho}} \tag{1}$$

In the case of static testing (V=0), thrust and torque were measured at different propeller rotational speeds. The propeller power can be calculated by:

$$P = 2\pi nQ \tag{2}$$

The thrust, torque and power coefficients of the propeller were calculated by

$$C_T = \frac{T}{\rho n^2 D^4} \ , \ C_q = \frac{Q}{\rho n^2 D^5} \ , \ C_p = \frac{P}{\rho n^3 D^5} \tag{3}$$

The static performance of the different propellers can be judged by static efficiency which is presented in the form of the figure of merit FoM [7] FoM usually is used to allow comparing the propeller static performance, and also used to measure the efficiency of helicopter rotors. It can be defined as:

$$FoM = \frac{C_T^{\frac{3}{2}}}{\sqrt{2}C_p} \tag{4}$$

For the dynamic testing, thrust and torque are measured at different values of advance ratio, which is defined as:

$$J = \frac{V}{nD} \tag{5}$$

Then, the power calculated as in equation(2). Also, the dynamic thrust, torque and power coefficients are calculated as in equation(3). At the end of the experiment, the three performance coefficients defined above are typically plotted against the advance ratio.

In the case of dynamic performance test, the propeller efficiency also plotted against the advance ratio, and it can be defined as:

$$\eta = \frac{TV}{P} = \frac{C_T}{C_p} J \tag{6}$$

The thrust and power coefficients curves, as presented in [2], show a small changes with the propeller RPM. In our simulation of the propeller-propulsion model, these changes are neglected.

Test Procedure

Before starting the test, the Sting balance must be calibrated. For this reason a six- component calibration test rig that shown in Fig. 12 was designed and manufactured to calibrate the sting balance. The calibration is conducted by applying a defined loads and acquiring the signal from the strain gauges. The calibration bar which contains the location of the applied load is mounted on the sting balance. Then the calibration test rig was leveled by adjusting the 4 screws at the bottom. The level was checked by a water balance. The calibration process starts by applying different loads (ranging from 50 g up to 4.5 kg). The corresponding micro strain

is measured and the calibration equation is deduced. This process is repeated for all sting balance components. The result of thrust and torque calibration are shown in Fig.13. Finally the calibration is checked by applying a pre-defined loads and comparing its value with the WT software readings.

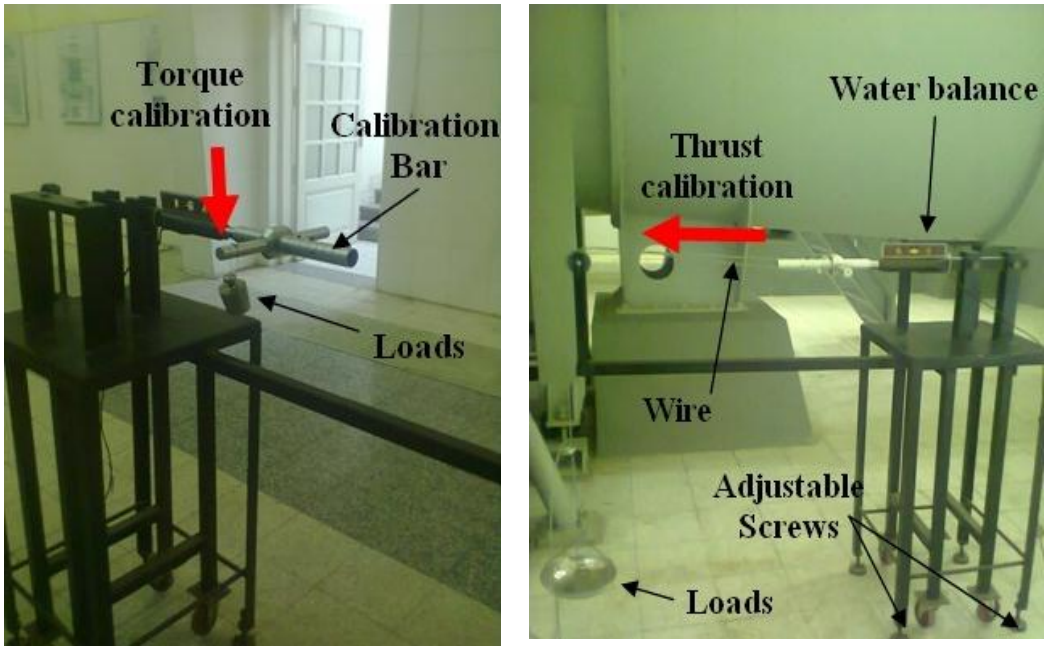

Fig. 12 Sting balance calibration test rig

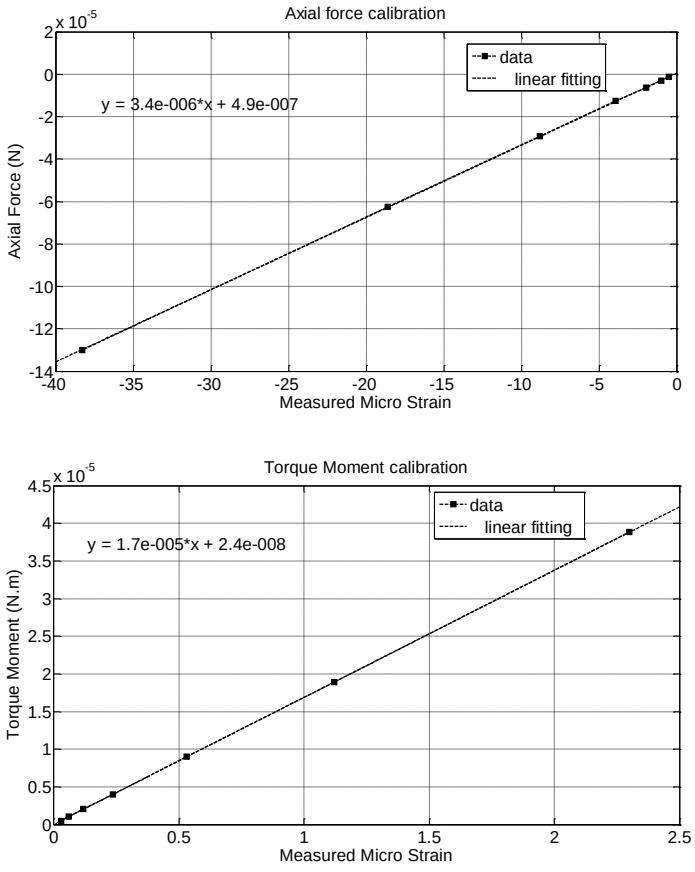

Fig.13. Thrust and torque moment calibration

Then the test rig, including all sensors, is installed inside the test section as shown in Fig. 14. The sting balance is powered about 20 minutes before measurements. This warming-up period is recommended by the manufacturer to allow the preheating of the strain gauges for stable measurements. With both the engine and wind tunnel are turned off, the tare values from the strain gauge are acquired to be subtracted from the measured data. Thrust, torque, pressure and temperature are recorded by the WT software. While the propeller speed and throttle position are recorded by the Eagletree system software. Before starting the experiment, the throttle position is calibrated and also the RPM sensor is calibrated for one magnet. The static and dynamic data are acquired to measure the propeller performance. For the static test (at zero wind speed), the propeller motor is set to the minimum speed. After the system reaches steady state, all sensor readings are acquired at this RPM. Then the process is repeated for increased values of rotational speed until reaching maximum RPM. Data sets are collected for approximately 16 rotational speeds ranging from: 5000 up to 12500 RPM. From the measured thrust and torque at each RPM, the thrust, torque, power coefficients and the static efficiency (FoM) are obtained and plotted versus the propeller rotational speed.

For the dynamic test, two methods are used to sweep the advance ratio. In the first one, the wind tunnel speed kept constant while throttle position is set to the minimum setting (corresponding to certain RPM). After the system reach steady state, all sensor readings are acquired. Then the throttle position is changed. This process is repeated until reaching the maximum allowable RPM. Data are collected for approximately 14 rotational speeds. While for the second method, throttle position is kept fixed and the wind tunnel airspeed set to the minimum. After the system reaches steady state, all sensor readings are acquired. Then, the wind tunnel airspeed is changed. This process is repeated until reaching the maximum wind tunnel speed. From the measured parameters, thrust, torque and power coefficient and efficiency could then be obtained and plotted versus the advance ratio. Data are collected for approximately ten airspeeds.

Fig. 14 Test rig inside the wind tunnel

Results of Propeller Test

Static Test Results

The static performance data are plotted against RPM including the thrust, torque, power coefficient and FoM as shown in Fig. 15. Results show that, the static coefficients and Figure of Merit can be considered constant with a very good accuracy over the tested range of RPM as shown in Table 2.

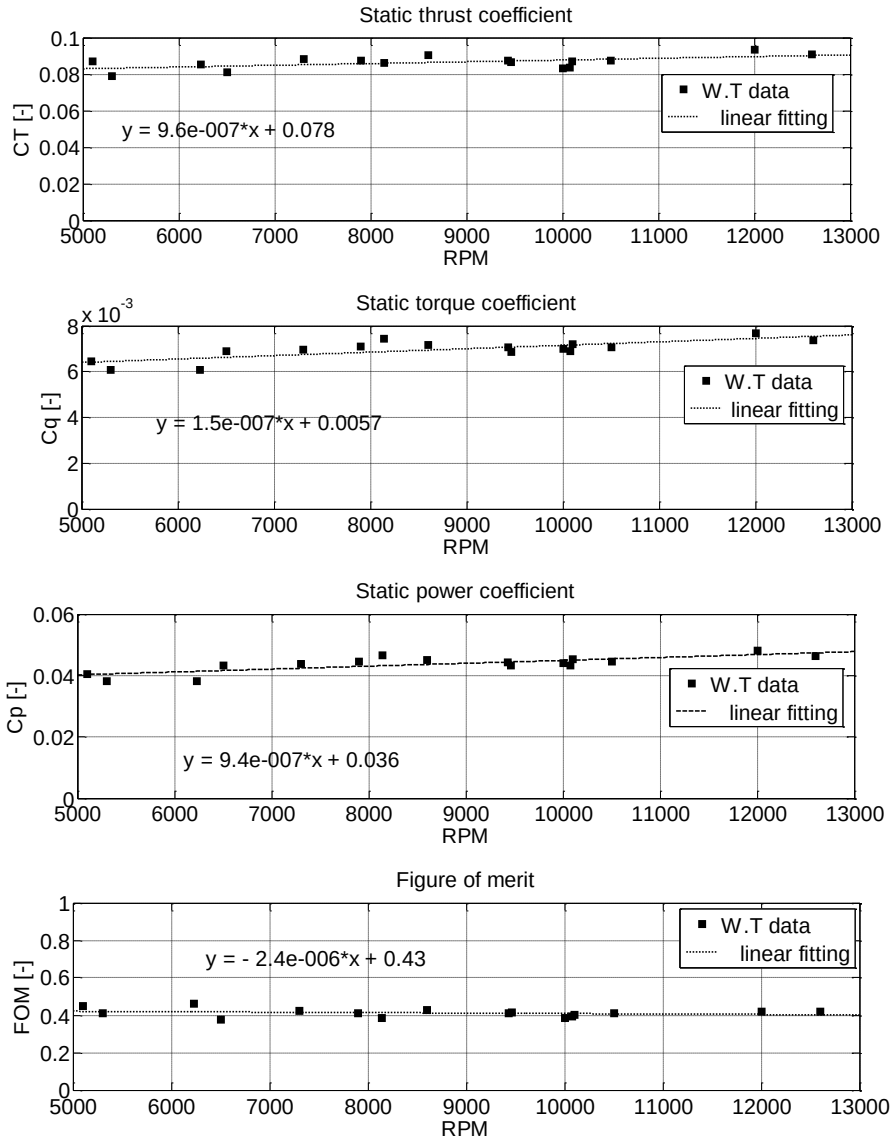

Fig. 15 Static propeller characteristics (linear fitting)

Table 2 Average normalized error for static characteristics

	Thrust coefficient	Torque coefficient	Power coefficient	Static efficiency (FoM)
Average error	0.01139	0.0010919	0.0068607	0.082187

Dynamic Test Results

The dynamic performance data are plotted against the advance ratio including four figures for thrust, torque, power coefficients and efficiency as shown in Fig. 16. The coefficients of thrust, torque and power decreases with advance-ratio. The propeller efficiency increases to maximum then decreases. Due to the limitation on minimum wind tunnel speed (approximately 23 m/s) and maximum propeller RPM (approximately 12500), the performance data could not be measured at values of advance ratio less than 0.5. To get the values of propeller coefficients at the whole range of advance ratio, all data are represented by the best polynomial fitting, and the norms of residuals are shown Table 3.

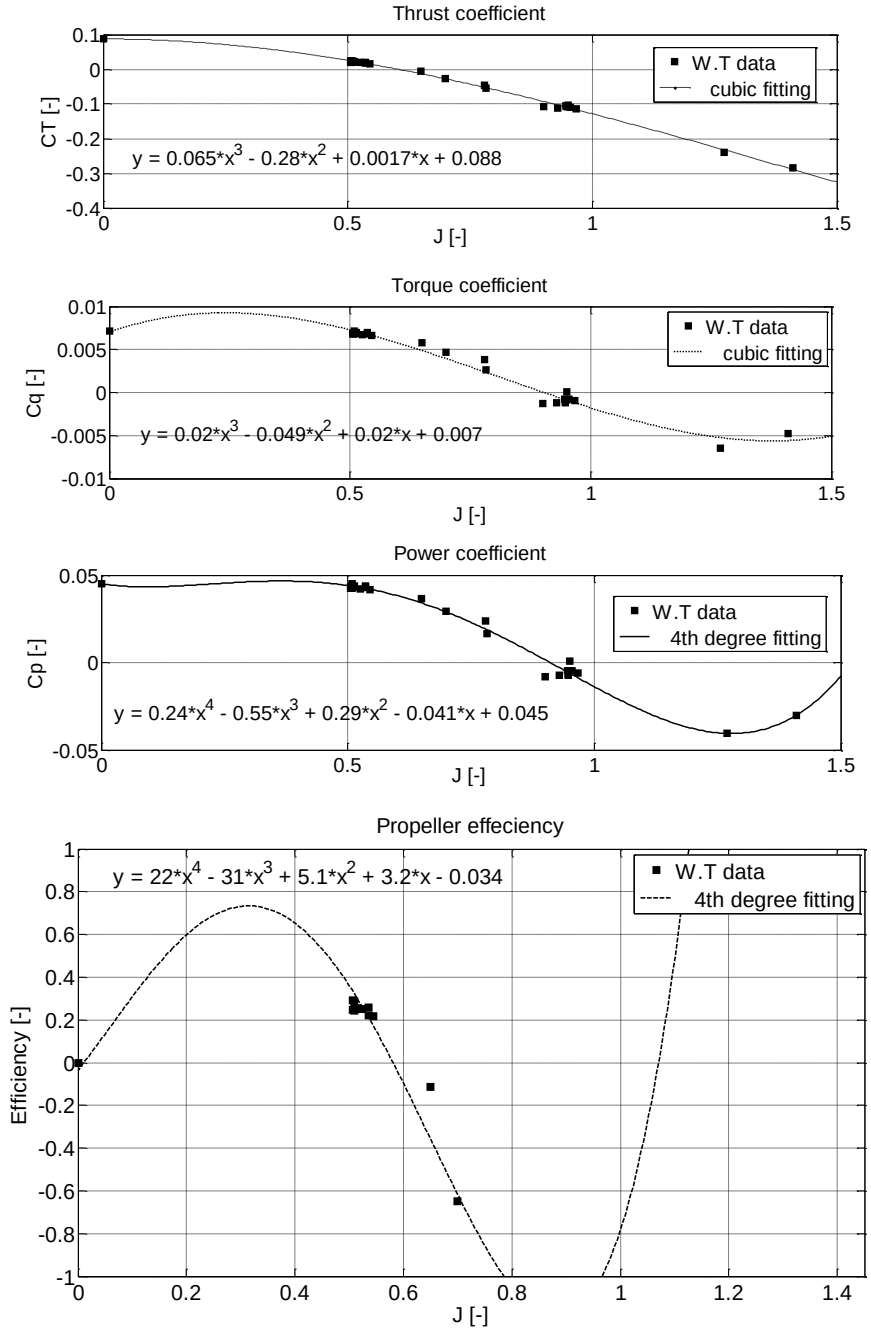

Fig. 16 Dynamic propeller characteristics (best fitting)

Table 3 Average normalized error for dynamic characteristics

	Thrust coefficient	Torque coefficient	Power coefficient
Average error	0.024943	0.0031237	0.014847

From the dynamic performance curves, it is clear that at nearly advance ratio (J=0.6), the thrust equals zero, and for larger value of (J), the thrust is negative (airbrake region). At nearly (J=0.9) power equals zero and for larger (J), the power is negative (wind mill region). From the efficiency curve, it can be found that the maximum efficiency equals approximately (0.73) at J near (0.31). Also it is clear that once the thrust goes negative, the efficiency is meaningless.

Validation of Measured Propeller Characteristics

In order to validate the measured static and dynamic performance data, they are compared to the results published in [5] For the static test, although the data in [5] are tested at a low RPM range from: 2000-6400, and the present data range (5000-12500), it is clear from Fig. 17 that there exist a very good agreement in the common RPM range (5000-6400)

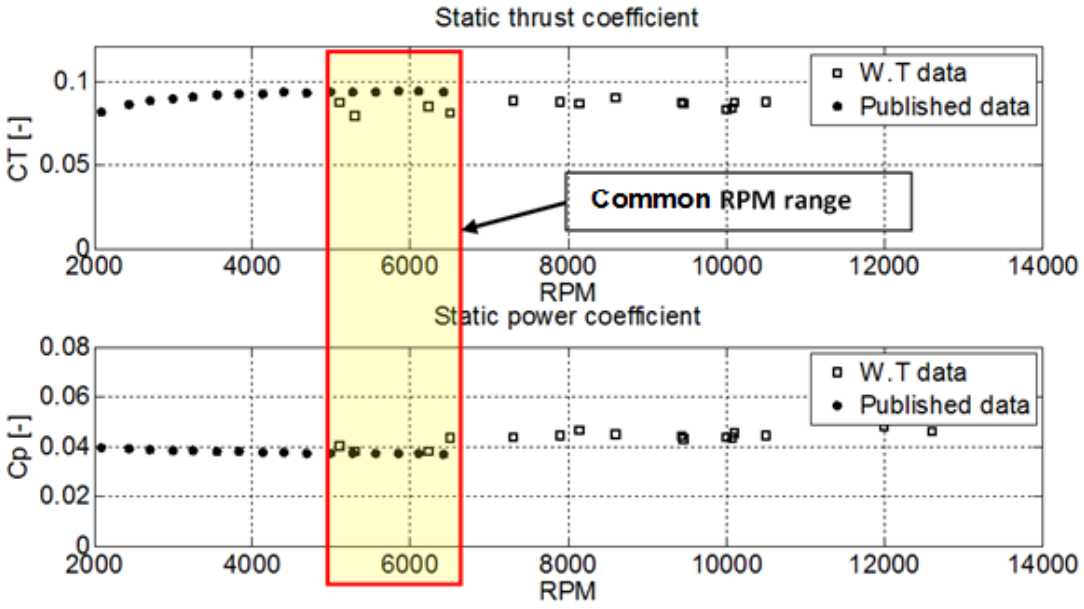

Fig. 17 Validation of static performance data

For the dynamic test, the agreement between the measured and published data is excellent for the thrust coefficient. For the power coefficient, while the measured and published data have the same trend, there is a very small noticeable difference, Fig. 18. This difference may be explained by noting that the published data in reference [5] are tested at fixed RPM (6000) while the measured experimental data collected at different RPM (5000-12500).

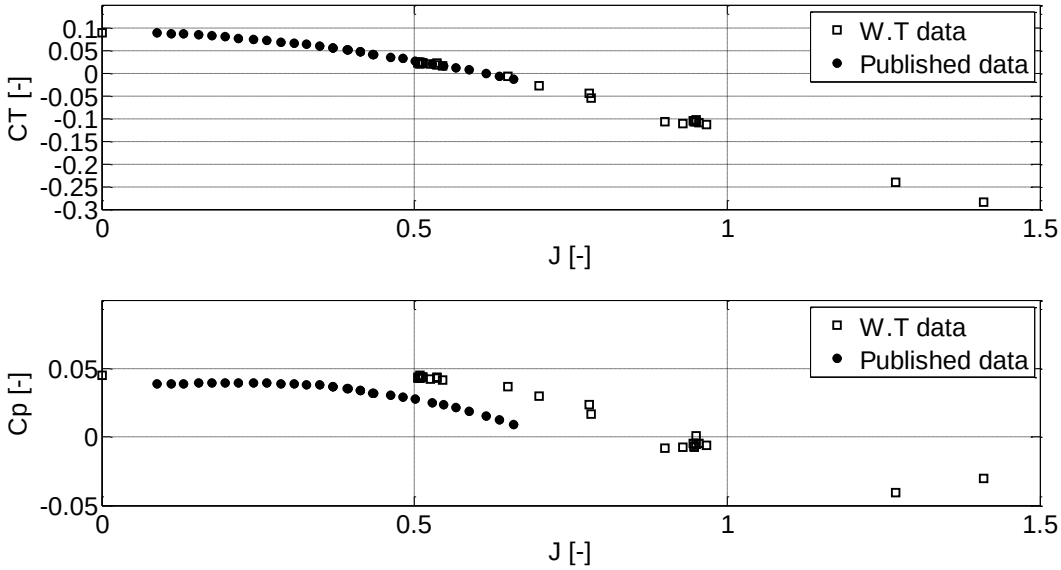

Fig. 18 Comparison between measured and published dynamic data [5]

Identification of the Piston Engine with its Servo

Piston engine dynamics are function of throttle and other several environment parameters such as: fuel inlet, manifold pressure, ambient temperature and air pressure which are difficult to measure. To simplify the engine and servo motor modeling, the engine and servo motor dynamic model can be identified based on experimental measurements for the input throttle position and the output engine RPM with time at zero wind tunnel airspeed. The same test rig described in section 2 is used. Finite pulses throttle input with variable widths are fed to the engine, then FDR is used to acquire the throttle position and the output RPM with frequency 10 Hz. A first and second order engine and servo motor models are identified by feeding the normalized input and output data into the Matlab System Identification Toolbox.

First Order Model

The initial conditions of the identified model are the minimum throttle configuration. The transfer function of the best fitting model for the first order found by the initial guess of the Matlab System Identification Toolbox is

$$G(s) = \frac{K}{Ts+1} \tag{7}$$

where $K = 4945, \quad T = 0.3418$

The measured data are first normalized with the maximum RPM value ($K = 4945$). To minimize the error between the measured output and the identified one, a Matlab code is developed to minimize the Mean Squared Error (MSE) to get the optimum transfer function parameter (time constant) for the normalized RPM. The code starts an iterative process from (0.5 to 2.5) of the above estimated parameters with step (0.001 *T*) until finding the optimum parameter as shown in Fig. 19.

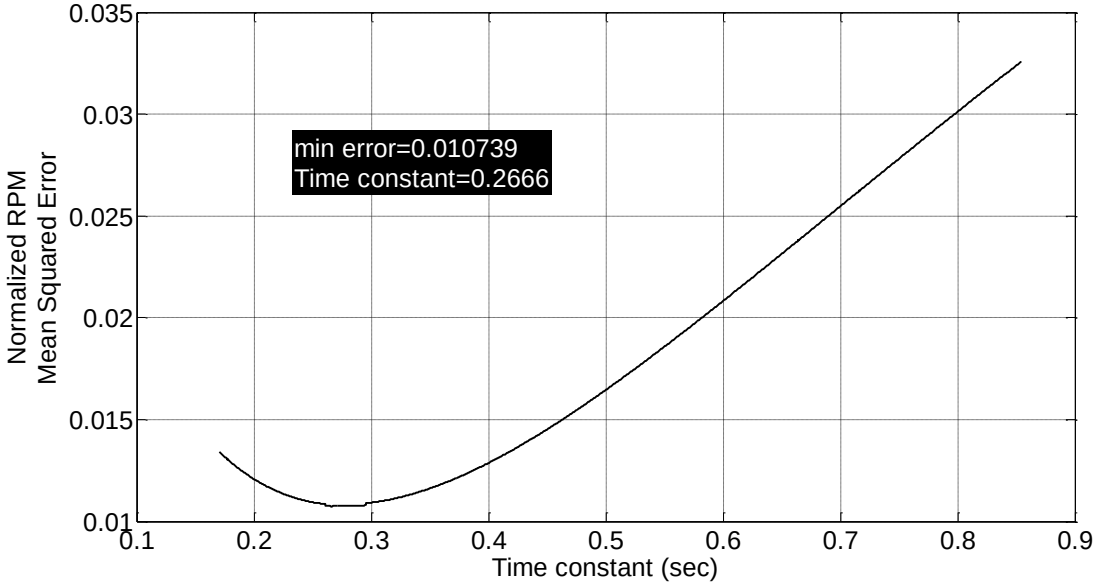

Fig. 19 Result of optimization process for the first order system

The results from the optimization process for the first order system are

$$T = 0.2666 \text{ , Min.Error= } 0.010739$$

Second Order Model

For second order system model, the transfer function of the best fitting model found by the initial guess of the Matlab System Identification Toolbox is

$$G(s) = \frac{K}{\left(\frac{s}{\omega_n}\right)^2 + \left(\frac{2\zeta}{\omega_n}\right)s + 1} \tag{8}$$

where: $\omega_n = 5.5460$, $\zeta = 0.8565$

To minimize the error between the measured output and the identified one, the same Matlab code is modified to be used for the second order system to get the transfer function parameters (ω_n, ζ) corresponding to minimum mean square error. The code starts an iterative process around the above estimated parameters, for the damping coefficient (from 0.5 to 1.5 of the above estimated value with step 0.005) and for the natural frequency (from 0.5 to 1.5 of the above estimated value with step 0.1) until finding the optimum parameters, Fig. 20.

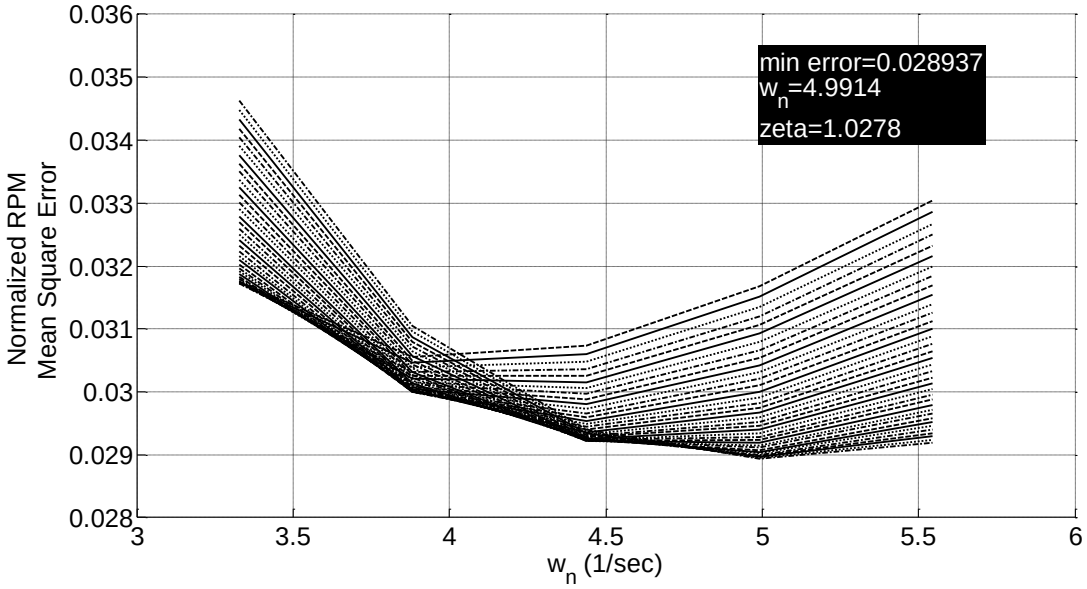

Fig. 20 Result of optimization process for the second order system

The results from the optimization process for the second order system are

$$\omega_n = 4.9914 \ , \zeta = 1.0278, \quad \text{Min.Error=0.028937}$$

Comparison and Validation of the Engine-Servo Model

Comparing first and second orders results shown in Table 4, it is clear that the error of first order system is smaller

Table 4 comparison between the engine models

Identified model	Mean square error (in normalized RPM)	Model parameters
First order model	0.010739	$K = 4945 \ , \ T = 0.2666$
Second order model	0.028937	$K = 4945 \ , \ \omega_n = 4.9914 \ , \zeta = 1.0278$

To validate the engine and its servo model, a set of full range of finite pulses with constant amplitudes are input to the real engine, and the output RPM is compared to the output from the identified first and second order models. As expected from the previous analysis, the first order model estimates the output of the engine better as shown in Fig. 21. So, the first order model is selected for representing the engine and its servo dynamics.

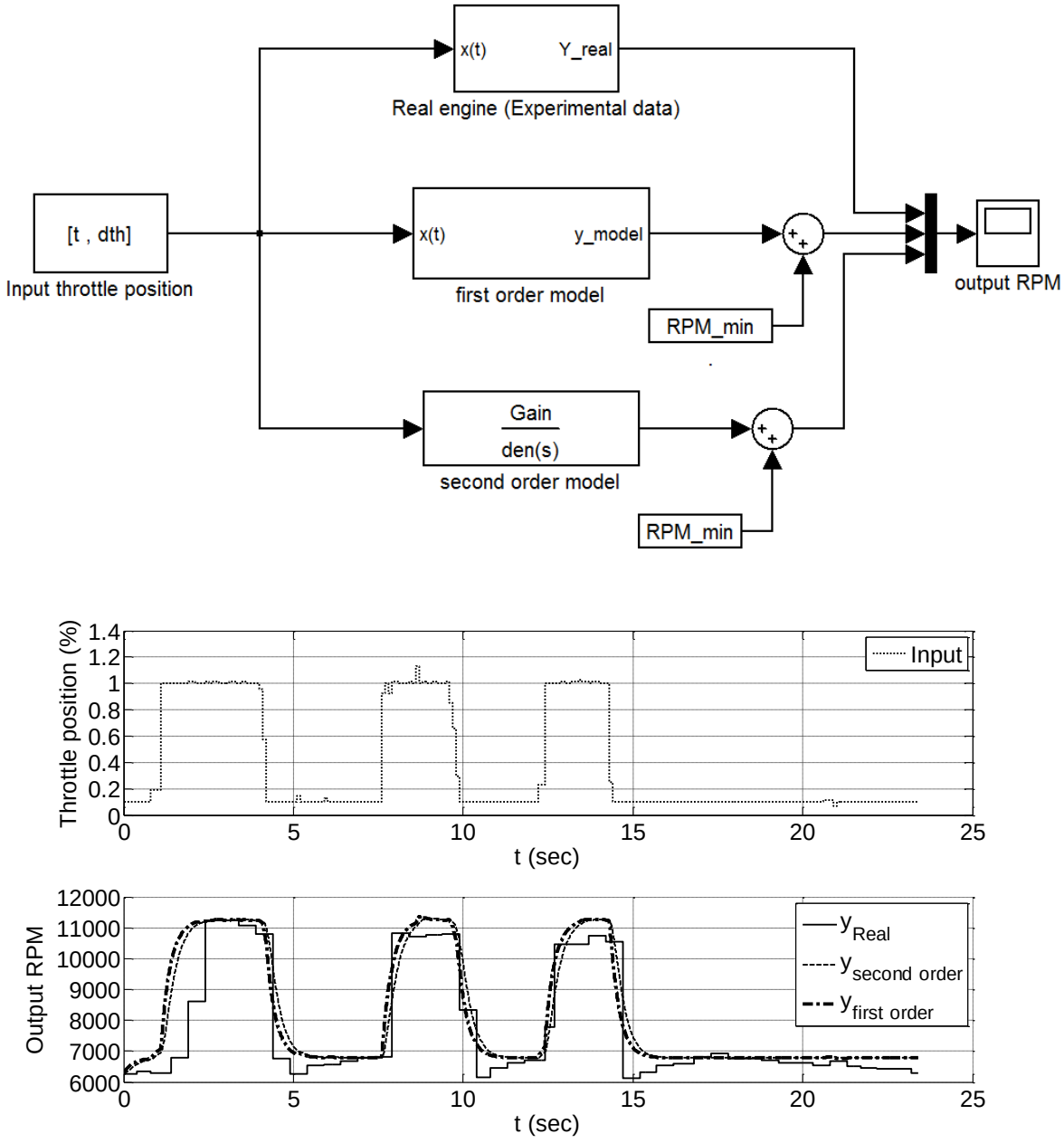

Fig. 21 Comparison between the measured and the identified outputs

Simulation of the Piston-Propeller Propulsion Model

The complete simulation of the piston-propeller propulsion model consists of the engine-servo model, which is represented by the obtained first order transfer function, and the propeller model, which is represented by the obtained dynamic performance characteristics. Matlab/Simulink is used to develop the simulation program of the propeller-propulsion model. As shown in Fig. 22, the model is able to estimate the thrust and torque at any throttle position input for a given flight conditions (speed and altitude). The thrust and torque are calculated according to the following relations:

$$T = C_T \rho n^2 D^4 \quad , \quad Q = C_q \rho n^2 D^5 \tag{9}$$

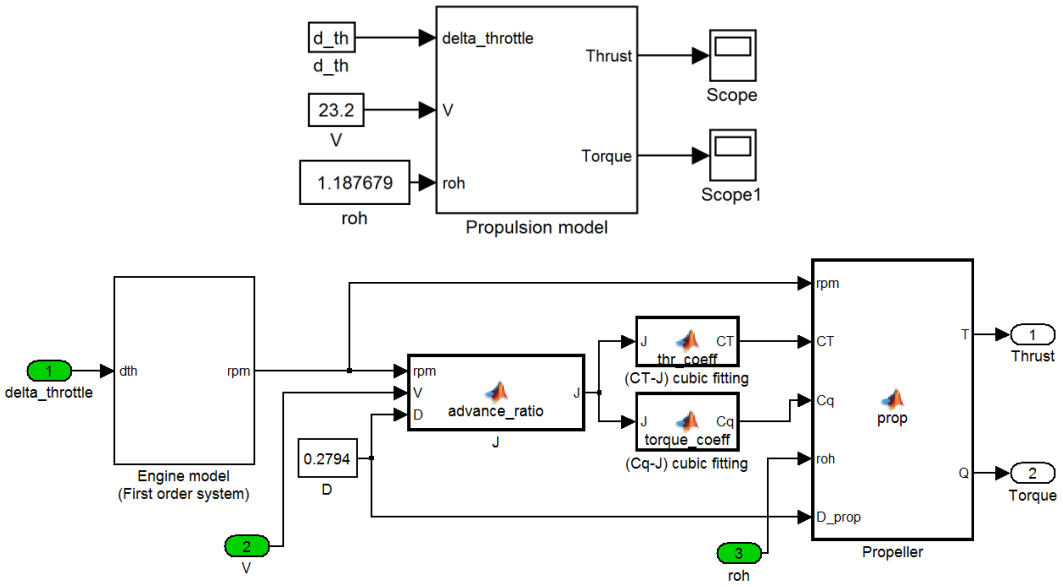

Fig. 22 Simulation diagram of the piston-propeller propulsion model

To validate the piston-propeller propulsion model, an experiment is conducted to measure the change of steady state thrust and torque with a given range of throttle position inputs at certain flight conditions (flow speed, pressure and temperature). The same throttle positions are fed to the Simulink propulsion model at the same flight conditions. The steady state simulation outputs (thrust and torque) are plotted against the experimental ones, Fig. 23.

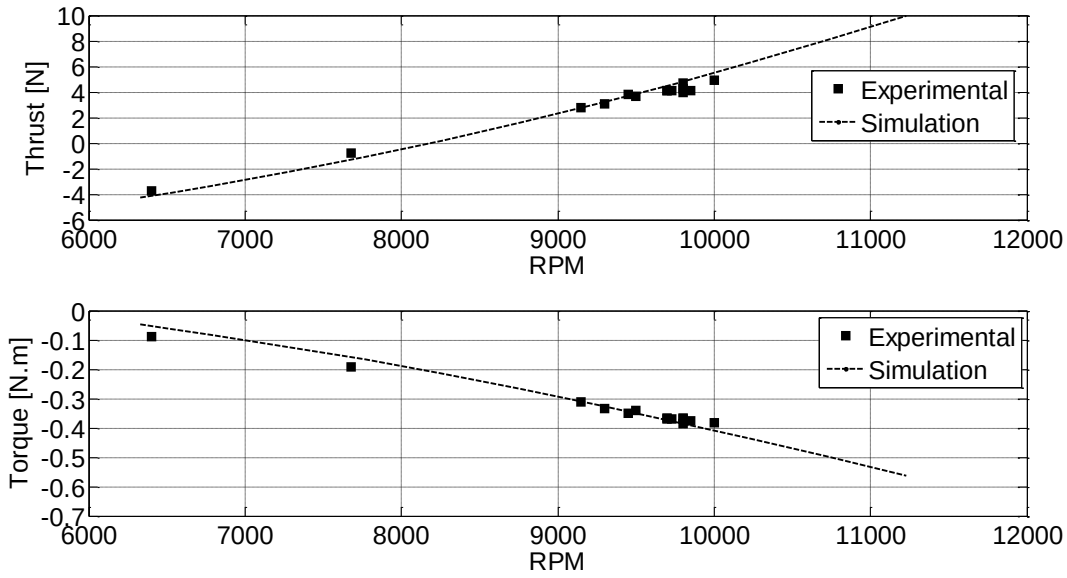

Fig. 23 Comparison between the experimental and simulation steady state values of thrust and torque versus RPM

It is clear from Fig. 23 that the agreement between the experimental and simulation data for both thrust and torque are very good. So the proposed propeller-propulsion model can be used to estimate the thrust and torque for any input throttle position.

Conclusion

In this paper, the propeller-propulsion model for the selected engine, propeller and servo motor is investigated based on experimental results from wind tunnel tests. Full propeller static and dynamic characteristics are measured and compared with experimental published data for the same propeller. A detailed experimental setup and procedure for both cases are presented. The comparison results show a very good agreement with static thrust, static power and dynamic thrust coefficients while there is a small difference in the dynamic power coefficient, which may be due to the fixed RPM of the engine at which the published data was measured. Also, it could be due to manufacturing differences between propellers. The engine-servo motor model is identified by a first and second order models. An optimization code is developed to compare the two models with measured data and find model parameters corresponding to the minimum MSE. Then, the first order model is selected to represent the engine dynamics. The complete propeller-propulsion simulation model is developed including the engine-servo model and the propeller performance map. An adequate simulated thrust and torque have been obtained.

Acknowledgement

The authors would like to thank A. M. Elashmawy at the aircraft mechanical department for his assist in the experimental tests.

References

[1] Kailash Kotwani., S.K. Sane., Hemendra Arya., K. Sudhakar., "Experimental Characterization of Propulsion System for Mini Aerial Vehicle", "*31st National Conference on FMFP*", *December 16-18, 2004.*

[2] Robert W. Deters., Michael S. Selig., "Static Testing of Micro Propellers", "*26th AIAA Applied Aerodynamics Conference*", 18 - 21 August 2008, Honolulu, Hawaii

[3] John B. Brandt., Michael S. Selig., "Propeller Performance Data at Low Reynolds Numbers", "*49th AIAA Aerospace Sciences Meeting*", 4-7 January 2011, Orlando, FL

[4] Amer AI-Radaideh, M.A.AI-Jarrah, Ali Jhemi, and R.Dhaouadi., "Arf60 Aus-Uav Modeling, System Identification, Guidance And Control: Validation Through Hardware In The Loop Simulation", "*Proceeding ofthe 6th International Symposium on Mechatronics and its Applications (ISMA09)*", Sharjah, UAE, March 24-26,2009

[5] Selig, M. "UIUC Propeller Database", 2012. http://www.ae.illinois.edu/m-selig/props/propDB.html .

[6] Wind tunnel reference manual.

[7] Leishman, J.G., "Principles of Helicopter Aerodynamics," Cambridge University Press, Cambridge, 2000.

[8] Hepperle, M., PropellerScanner Manual, http://www.mh-aerotools.de , 2003.